Ceramics International

Submitted March 20th, 2015

Revised May 12th, 2015

Properties of aerosol deposited NASICON-type $Li_{1.5}Al_{0.5}Ge_{1.5}(PO_4)_3$ solid electrolyte thin films

Ryoji Inada*, Kei-ichi Ishida, Masaru Tojo, Takayuki Okada, Tomohiro Tojo, and Yoji Sakurai

Department of Electrical and Electronic Information Engineering, Toyohashi University of Technology, 1-1 Hibarigaoka, Tempaku-cho, Toyohashi, Aichi 441-8580, Japan.

*Corresponding author

Ryoji Inada, Associate Professor

Postal address: Toyohashi University of Technology, 1-1 Tempaku-cho, Toyohashi, Aichi 441-8580, Japan

Phone: +81-532-44-6723

Fax: +81-532-44-6757

E-mail address: inada@ee.tut.ac.jp

Abstract

NASICON-type $Li_{1.5}Al_{0.5}Ge_{1.5}(PO_4)_3$ (LAGP) solid electrolyte thin film was fabricated without any heat treatment by aerosol deposition (AD). Ball-milled LAGP powders with different particle sizes were used as raw material and deposited directly on a stainless steel substrate via room temperature impact consolidation. X-ray diffraction patterns revealed that as-deposited LAGP film has a same crystal structure with raw LAGP powder and no secondary phases are formed during deposition. SEM observation showed that film consists of fractured LAGP nanoparticles but the porosity is strongly influenced by an averaged particle size of raw LAGP powder. Maximum total (bulk + grain-boundary) ionic conductivity at room temperature in aerosol deposited (ADed) LAGP film was 0.5×10^{-5} S cm^{-1}, while the bulk conductivity of film is approximately 10^{-4} S cm^{-1}, which is comparable with the bulk property of LAGP as previously reported. Therefore, lower total conductivity of ADed LAGP film is mainly attributed to large grain-boundary resistance between the LAGP nanoparticles in the film. Improvement of film density and the connectivity among the LAGP nanoparticles in the film should be needed to enhance the total conductivity.

Keywords: $Li_{1.5}Al_{0.5}Ge_{1.5}(PO_4)_3$; Solid electrolyte; Thin film; Aerosol deposition; Ionic conductivity

1. Introduction

All-solid-state lithium-ion batteries (LiBs) are expected as one of the next generation energy storage devices because of their high energy density, high safety and excellent cycle stability [1–3]. Development of solid inorganic lithium-ion conducting materials used as solid electrolyte is the most important issue for realization of all solid-state LiBs. The materials used for solid electrolyte must have not only high lithium-ion conductivity $\sigma_{Li} > 10^{-3}$ S cm^{-1} at room temperature but also chemical stability against metallic lithium or lithiated negative electrode, air and moisture. Although oxide based solid electrolytes have rather lower σ_{Li} than sulfide based one, they have other advantages such as their chemical stability and easiness for handling.

Among various oxide based solid electrolytes, $Li_{1.5}Al_{0.5}Ge_{1.5}(PO_4)_3$ (LAGP) [4–10] with NASICON-type framework has several advantages over other electrolytes such as $Li_{1+x}Al_xTi_{2-x}(PO_4)_3$ (LATP) [11–13], $Li_{2/3-3x}La_xTiO_3$ (LLT) [14–17] and $Li_7La_3Zr_2O_{12}$ (LLZ) [18–21]. Although LATP have also NASICON-type structure and higher σ_{Li} than LAGP, LAGP has a wider electrochemical potential window than LATP which reacts with Li at ~2.4 V vs. Li/Li$^+$ due to the Ti^{4+}/Ti^{3+} redox reaction [6, 9]. Perovskite-type LLT has much higher bulk ionic conductivity than LAGP, but very high temperature sintering above 1400°C must be applied for densification and reduction of grain-boundary resistance [15]. In addition, LLT also reacts with Li at ~1.7 V vs. Li/Li$^+$ due to the Ti^{4+}/Ti^{3+} redox reaction [16, 17]. Such narrow electrochemical stability window for LATP and LLT gives a difficulty to use them in a practical use for solid-state LiBs. Compared to garnet-type LLZ solid electrolytes, LAGP can be easily synthesized without any phase transition during synthesis condition such as heat-treatment temperature and elementary composition [18–21]. σ_{Li} of sintered LAGP is ~10^{-4} S cm^{-1} at room temperature and at

least one digit lower than organic liquid electrolyte. This property has not been regarded as high enough for practical use in all-solid-state batteries operating at room temperature.

Solid electrolyte thin film provides low electrical resistance, small size of a device and increasing volumetric energy density for all-solid-state battery. Several studies have been carried out for preparing thin film solid electrolyte using RF magnetron sputtering [22–25], pulsed laser deposition [26, 27] and sol-gel methods [28–30]. These methods are efficient for fabricating uniform film and controlling the film thickness, but in some cases, it is difficult to control elementary composition. Moreover, increasing substrate temperature during deposition and/or post-annealing should be necessary to obtain well-crystallized thin films. Since high temperature treatments may lead to undesired reactions at the interface or uncontrolled diffusion between electrode and solid electrolyte, these methods are not recommended in some cases and inadequate for fabricating all-solid-state batteries.

Aerosol deposition (AD) has many advantages compared to other conventional thin film deposition methods as mentioned above, including deposition of a crystallized thin film without any heat treatments and a fast deposition rate [31–33]. A film is deposited through impact and adhesion of fine particles on substrate at room temperature. This phenomenon is called as “room temperature impact consolidation (RTIC)” (Fig. 1). Consequently, as-deposited film has similar properties with raw powder material, such as the crystal structure, composition and physical property. AD additionally provides a number of advantages, including room temperature deposition and high adhesion strength with a substrate [31–33]. By addressing these attractive features, numerous studies to form thin film by using AD have been reported in various functional ceramic materials, including $Pb(Zr,Ti)O_3$ (PZT) [32, 33], $(K_{0.5}Na_{0.5})NbO_3$ [34], TiO_2 [35], and $Ca_3Co_4O_9$

films [36]. Several papers have been also reported in the battery field. Popovici et al. reported the adoption of AD to prepare LATP solid electrolyte film and the as-deposited film showed total conductivity of 1.1×10^{-6} S cm^{-1} at 22ºC [37]. Ahn et al. also reported the properties of LLZ solid electrolyte film fabricated by AD without any heat treatment, but the conductivity is 10^{-8} S cm^{-1} even at 140ºC [38], which is much lower than sintered LLZ [18]. The electrochemical properties of Si alloy or composite [39–42], $LiMnO_2$ [43], $LiNi_{1/3}Co_{1/3}Mn_{1/3}O_2$ [44, 45], $LiFePO_4$ [46], $Li_4Ti_5O_{12}$ [47] and Fe_2O_3 [48] film electrodes were also investigated to verify the feasibility of AD.

In this paper, we fabricated NASICON-type LAGP solid electrolyte thin film by AD. Although LAGP is not stable against lithium metal [10], it has a much wider electrochemical potential window than LATP and LLT. For constituting all-solid-state LiB using LAGP, several anode materials operating at high potential for lithium-ion storage such as $Li_4Ti_5O_{12}$, TiO_2 and Nb_2O_5 can be potentially used. LLZ is known to be stable against lithium metal and have better electrochemical stability than LAGP, but synthesis of LAGP is much easier than LLZ. Furthermore, fabrication of LATP film with NASICON-type crystal structure has been demonstrated in [37], so that we selected LAGP as the materials for fabrication of solid-electrolyte thin film by AD. LAGP powders with different particle sizes were directly used as raw material for LAGP film formation via RTIC. The crystallinity, microstructure and ionic conductivity of as-deposited LAGP film without any heat treatment were investigated.

2. Experimental

LAGP powder was prepared by a conventional solid state reaction method. Stoichiometric amounts of Li_2CO_3 (Kojundo Chemical Laboratory Co., Ltd., 99.99%), γ-

Al_2O_3 (Kojundo Chemical Laboratory Co., Ltd., 99.9%), GeO_2 (Kojundo Chemical Laboratory Co., Ltd., 99.99%), and $NH_4H_2PO_4$ (Nacalai Tesque Inc., 99%) were ground with acetone in an agate mortar, and then calcined at 450°C for 20 h in Pt-Au5% alloy crucible. The calcined powders were ground again and pressed into pellets. Finally, the pellets were annealed at 950°C for 10 h in air using Pt-Au5% alloy crucible.

It has been reported that both size and morphology of raw powder are important factors for structure and property of an ADed film [27, 45, 47]. In order to prepare LAGP powders with different particle size, as-synthesized LAGP powder was pulverized using planetary ball-milling (Nagao System, Planet M2-3F) with ethanol and zirconia ball (2 mm in diameter) for different milling time of 3 h and 4.5 h. Rotation speed of planetary ball-milling was fixed to 300 rpm. Obtained LAGP powders with different milling time were used as raw material for fabrication of LAGP film.

Schematic illustration of AD apparatus is shown in Fig. 2. It consists of a carrier gas supply system, an aerosol chamber, a deposition chamber equipped with a motored *X*–*Y*–*Z* stage and a nozzle with a thin rectangular shaped-orifice with the size of 10 mm × 0.5 mm. Deposition starts with evacuating deposition chamber. A pressure difference between carrier gas system and deposition chamber is generated as a power source for film deposition. A carrier gas flows out from gas supply system to aerosol chamber. In aerosol chamber, powder is dispersed into carrier gas with no agglomeration. Finally, well dispersed aerosol flows into deposition chamber through a tube and is sprayed onto substrate. Stainless steel SUS316L plate with a thickness of 0.2 mm was used as a substrate. The deposition area was masked into a square shape with an area size of 10 × 10 mm^2. Nitrogen (N_2) gas was used as a carrier gas. Deposition chamber was evacuated to a low vacuum state around 10 Pa and deposition was carried out for 20 minutes. During

deposition process, the stage was moved uni-axially with back-and-forth motion length of 50 mm. Distance between tip of nozzle and substrate was set to be 10 mm. According to our previous study for ADed $Li_4Ti_5O_{12}$ film [47], mass flow of N_2 carrier gas was fixed to 20 L min^{-1}. Simple tape testing was also carried out to confirm the adhesion between as-deposited LAGP film and substrate. Kapton® tape was put on to the film and then it peeled, but film exfoliation was not occurred.

Crystal structure of both LAGP powders and ADed LAGP film was evaluated by X-ray Diffractometer (MultiFlex, Rigaku) using CuKα radiation (λ = 0.15418 nm), with measurement range 2θ = 5–90° and step interval of 0.04°. Field emission scanning electron microscope (FE-SEM, SU8000 Type II, Hitachi) was used to observe microstructure of both powders and ADed films. Ionic conductivity of ADed LAGP film was evaluated at 27°C and frequency from 5 Hz to 5 MHz with applied voltage amplitude of 0.1 V, using both Hioki Chemical Impedance Meter 3532-80 (for the measurement up to 1 MHz) and Hioki LCR Hightester 3532-50 (for the measurement from 1 MHz to 5 MHz). Before the conductivity measurements, one parallel surface of LAGP film was sputtered with Au with an area size of 0.8 × 0.8 cm^2, so that the film was sandwiched with SUS316L and Au as Li^+ blocking electrodes as shown in Fig. 3.

3. Results and discussion

XRD pattern for as-synthesized LAGP powder is shown in Fig. 4(a). Although very small amounts of GeO_2, $AlPO_4$ and $Li_4P_2O_7$ are included, all the main peaks for as-synthesized powder well match to the pattern for $LiGe_2(PO_4)_3$ (LGP) with NASICON-type structure [49], so that NASICON-type LAGP powder could be synthesized. 25% of Ge in LGP has been substituted by Al, but the diffraction peaks are not dramatically

shifted, due to the similarity in ionic radius between Ge^{4+} (0.053 nm) and Al^{3+} (0.050 nm). Fig. 4(b) shows SEM image of as-synthesized LAGP powder. Cuboid-shaped LAGP particles with the size of 2–3 μm are obtained.

Size and morphology of raw powder materials are one of the important factors for structure and property of ADed film. Moreover, we could not fabricate LAGP film using as-synthesized LAGP powders (Fig. 4(b)) as raw materials, so that as-synthesized LAGP powders were pulverized by ball-milling to control the particle sizes of LAGP suitable for AD. SEM images of ball-milled LAGP powders with different milling time of 3 h and 4.5 h are shown in Fig. 5(a) and (b), respectively. Compared with as-synthesized powder (Fig. 4(b)), the particle sizes of ball-milled LAGP powders are clearly reduced. Moreover, the averaged particle size is confirmed to be decreased monotonically with increasing milling time. The powders milled for 3 h (Fig. 5(a)) dominantly contain LAGP particles with the size of 0.5–1 μm while for the powders milled for 4.5 h (Fig. 5(b)), LAGP particles with the size of 0.3–0.5 μm are dominantly included and some of them are partially agglomerated. These two LAGP powders were directly used as raw materials for LAGP film fabrication by AD.

XRD patterns for ADed LAGP film on SUS316L substrate are shown in Fig. 6. For comparison, the patterns for LAGP powder is also plotted. The peaks from LAGP with NASICON-type structure are clearly observed in ADed LAGP film, together with the peaks from the substrate. This indicates that crystalline LAGP film was successfully fabricated without applying any heat treatments. The peaks from other secondary phases were not observed. This feature is a advantage over other conventional thin film deposition methods such as sputtering and sol-gel method, because by using these deposition methods, heat treatment such as heating substrate during deposition or post

annealing should be necessary to obtain well crystallized film [24–30]. However, it should be noted that the absolute value of peak intensity in raw LAGP powder is approximately 10 times larger than that for ADed LAGP film. In addition, the peaks for LAGP film becomes broader than those for LAGP powder used as raw material. Similar phenomenon has been confirmed in other ADed films [31–38, 44, 46, 48].

Fig. 7 shows SEM images of surface (left) and cross-section (right) of ADed LAGP films using two different LAGP powders as shown in Fig. 5. It is confirmed that both films consist of fractured LAGP particles with the size around 100 nm. Fracturing raw LAGP powders during AD process is one of the main reasons for broadening the diffraction peaks of ADed LAGP films as mentioned above. The film using 3 h-milled powder (Fig. 5(a)) has denser structure than the film using 4.5 h-milled powder. Relative film densities calculated from the theoretical density of LAGP (= 3.42 g cm^{-3}) [9] were estimated to be approximately 80% for the former while 65% for the latter, which is consistent with SEM observation results (Fig. 7). In addition, the thickness of the former (= 10 μm) is slightly larger than the latter (= 6 μm). Since the deposition parameters during AD process such as mass flow of carrier gas, pressure of chamber during deposition and deposition time are identical, the difference in both microstructure and deposition rate among the films is caused by the difference in particle size and morphology of raw LAGP powders. In our previous work, we fabricated $Li_4Ti_5O_{12}$ (LTO) film by AD, using agglomerated powder with the size of 5–6 μm composed of primary sub-micron LTO particles as raw material [47]. ADed LTO film showed porous structure composed of LTO particles with the size of several 100 nm, which is similar to LAGP film using 4.5 h-milled powder as raw material. At present, the detail mechanism to cause the difference in microstructure of LAGP films due to size and morphology of raw LAGP

powders has not been fully clarified. However, it is evident that at least, well dispersed LAGP powder with the size of 0.5–1 μm (Fig. 5(a)) is more suitable to form denser LAGP film.

The conductivity of ADed LAGP films fabricated was examined by AC impedance spectroscopy. Nyquist plots of AC impedance measured at 27°C for ADed LAGP films are shown in Fig. 8. Here, Z' and Z'' are real and imaginary parts of impedance, respectively. For both LAGP films, semicircle and linear portion data were obtained in high and low frequency regions, indicating that the conducting nature of the film is primary ionic. Intercept point of linear tail in low frequency range with real axis nearly corresponds to total (bulk and grain-boundary) resistance R_{total}, while the intercept point between semicircle and real axis in high frequency range indicates bulk resistance R_{bulk} of LAGP particle consisting the film [9]. R_{total} of the film using 3 h-milled powders (Fig. 8(a)) is confirmed to be one digit lower than the film using 4.5 h-milled powders (Fig. 8(b)). As shown in Fig. 7, since the difference in film thickness among the films is not so large (10 μm and 6 μm), the total conductivity of the film using 3 h-milled powders is expected to be much higher than the film using 4.5 h-milled powders. Moreover, as shown in the insets in the graphs, the difference in R_{bulk} among the films seems to be small (5 Ω and 9 Ω), so that the large difference in R_{total} among the films is mainly attributed to the difference in grain-boundary resistance.

Bulk and total conductivity σ_{bulk} or σ_{total} for each ADed LAGP film can be calculated by R_{bulk} and R_{total} estimated from Fig. 8, area of Au electrode A (= 0.64 mm^2) on the film surface and thickness of each film shown in Fig. 7. As a result, we obtained $\sigma_{bulk} = 3.1 \times 10^{-4}$ S cm^{-1} and $\sigma_{total} = 0.5 \times 10^{-5}$ S cm^{-1} at 27°C for the film using 3 h-milled powders (Fig. 7(a)), while $\sigma_{bulk} = 1.0 \times 10^{-4}$ S cm^{-1} and $\sigma_{total} = 0.2 \times 10^{-6}$ S cm^{-1} at 27°C for the

film using 4.5 h-milled powders (Fig. 7(b)). σ_{total} in the former is more than one digit higher than the latter while σ_{bulk} is comparable among the films. As shown in Fig. 7, the latter has more porous structure and lower film density so that grain-boundary resistance of the latter is much larger than the former.

Maximum σ_{total} at room temperature of our LAGP film by AD is comparable with amorphous lithium phosphorous oxy-nitride (LiPON) film prepared by magnetron sputtering [22, 23], LLZ film by PLD method [26, 27] and LATP film by sol-gel method [28, 29] or AD [37], but more than one digit lower than sintered LAGP in the literature [3–8]. The values of σ_{bulk} at room temperature for sintered LAGP are reported to be in the range between 10^{-4} and 10^{-3} S cm^{-1}, so that our ADed LAGP films have much larger grain-boundary resistance than sintered LAGP while the degradation of σ_{bulk} by fracturing LAGP particles during AD process seems to be not so remarkable. Compared with sintered LAGP, the grain size in the film by AD is small, which increase the volume ratio between grains and grain-boundaries in the film. Both lower film density (80% as maximum in this work) and an increased volume ratio between grain and grain-boundaries could be considered as main reason to reduce the σ_{total} in ADed LAGP film. Further improvement of σ_{total} should be necessary for the application to all-solid state LiB, and we are currently trying to improve by increasing film density by optimization of powder treatments and deposition parameters such as mass flow of career gas and inclining angle of the nozzle against the substrate.

It is worth to note that LiPON [22, 23] and LLZ films [26] are stable even against lithium metal so that lithium metal and other various lithiated anode materials with them for fabricating solid-state battery. Since LAGP shows better electrochemical stability than LATP and LLT but reacts with lithium at the potential around 0.8–0.9 V vs. Li/Li^+ [10],

it is difficult to contact with lithium metal directly, which is needed for precise electrochemical stability measurement [26]. Therefore, we have not examine the stability of ADed LAGP film against lithium metal at present. However, the film fabricated by AD generally shows similar characteristic properties of raw powder material, such as the crystal structure, composition and physical property. Therefore, ADed LAGP film is expected to be not stable against lithium metal and anode materials with operating potential higher than lithium plating should be used for constituting solid-state battery.

4. Conclusion

NASICON-type LAGP solid electrolyte thin film was fabricated on SUS316 substrate by aerosol deposition (AD). LAGP powders were used as raw material and sprayed directly onto a substrate to form LAGP film without applying any heat treatments. XRD patterns revealed that aerosol deposited (ADed) LAGP film has a same crystal structure with raw LAGP powder and no secondary phases were formed during the film deposition. Porosity of ADed LAGP films is strongly influenced by the size of raw LAGP particles. Dense LAGP films consisting of fractured LAGP nanoparticles can be obtained using LAGP powders with an averaged particle size of 0.5–1 μm. Maximum total ionic conductivity at 27°C in ADed LAGP film was estimated to be 0.5×10^{-5} S cm^{-1}. Total conductivity is much lower than sintered LAGP, which is mainly due to larger grain-boundary resistance between fractured LAGP particles in the film.

Acknowledgements

This work was partly supported by JSPS KAKENHI Grant Number (Challenging Exploratory Research) 26630111 and Research Foundation for the Electrotechnology of

Chubu Grant Number R-25209.

References

[1] K. Takada, Progress and prospective of solid-state lithium batteries, Acta Mater. 61 (2013) 759–770.

[2] M. Tatsumisago, M. Nagao, A. Hayashi, Recent development of sulfide solid electrolytes and interfacial modification for all-solid-state rechargeable lithium batteries, J. Asian Ceram. Soc. 1 (2013) 17–25.

[3] S. Teng, J. Tan, A. Tiwari, Recent developments in garnet based solid state electrolytes for thin film batteries, Current Opinion in Solid State and Materials Science 18 (2014) 29–38.

[4] J. Fu, Fast Li^+ ion conducting glass-ceramics in the system Li_2O–Al_2O_3–GeO_2–P_2O_5, Solid State Ionics 104 (1997) 191–194.

[5] X. Xu, Z. Wen, X. Wu, X. Yang, Z. Gu, Lithium ion conducting glass-ceramics of $Li_{1.5}Al_{0.5}Ge_{1.5}(PO_4)_3$–$xLi_2O$ (x=0.0-0.20) with good electrical and electrochemical properties, J. Am. Ceram. Soc. 90 (2007) 2802–2806.

[6] C.R. Mariappana, C. Yada, F. Roscianoc, B. Rolinga, Correlation between micro-structural properties and ionic conductivity of $Li_{1.5}Al_{0.5}Ge_{1.5}(PO_4)_3$ ceramics, J. Power Sources 196 (2011) 6456–6464.

[7] H. Chung, B. Kang, Increase in grain boundary ionic conductivity of $Li_{1.5}Al_{0.5}Ge_{1.5}(PO_4)_3$ by adding excess lithium, Solid State Ionics 263 (2014) 125–130.

[8] J.K. Feng, B.G. Yan, J.C. Liu, M.O. Lai, L. Li, All solid state lithium ion rechargeable batteries using NASICON structured electrolyte, Mater. Technol. 28

(2013) 276–279.

[9] J. Yang, Z. Huang, B. Huang, J. Zhou., X. Xu, Influence of phosphorus sources on lithium ion conducting performance in the system of Li_2O–Al_2O_3–GeO_2–P_2O_5 glass–ceramics, Solid State Ionics 270 (2015) 61–65.

[10] J.K. Feng, L. Lu, M.O. Lai, Lithium storage capability of lithium ion conductor $Li_{1.5}Al_{0.5}Ge_{1.5}(PO_4)_3$, J. Alloys Compd. 501 (2010) 255–258.

[11] H. Aono, E. Sugimoto, Y. Sadaoka, N. Imanaka, G. Adachi, Ionic conductivity of the lithium titanium phosphate ($Li_{1+X}M_XTi_{2-X}(PO_4)_3$, M = Al, Sc, Y, and La) systems, J. Electrochem. Soc. 136 (1989) 590–591.

[12] H. Aono, E. Sugimoto, Y. Sadaoka, N. Imanaka, G. Adachi, Ionic conductivity of solid electrolytes based on lithium titanium phosphate, J. Electrochem. Soc. 137 (1990) 1023–1027.

[13] J. Fu, Superionic conductivity of glass-ceramics in the system Li_2O–Al_2O_3–TiO_2–P_2O_5, Solid State Ionics 96 (1997) 195–200.

[14] Y. Inaguma, C. Liquan, M. Itoh, T. Nakamura, High ionic conductivity in lithium lanthanum titanate, Solid State Commun. 86 (1993) 689–693.

[15] Y. Inaguma, M Nakashima, A rechargeable lithium-air battery using a lithium ion-conducting lanthanum lithium titanate ceramics as an electrolyte separator, J. Power Sources 228 (2013) 250–255.

[16] C.H. Chen, K. Amine, Ionic conductivity, lithium insertion and extraction of lanthanum lithium titanate, Solid State Ionics 144 (2001) 51–57.

[17] C. Hua, X. Fang, Z. Wang, L. Chen, Lithium storage in perovskite lithium lanthanum titanate, Electrochem. Commun. 32 (2013) 5–8.

[18] R. Murugan, V. Thangadurai, W. Weppner, Fast lithium ion conduction in garnet-

type $Li_7La_3Zr_2O_{12}$, Angew. Chem. Int. Ed. 46 (2007) 7778–7781.

[19] E. Rangasamy, J. Wolfenstein, J. Sakamoto, The role of Al and Li concentration on the formation of cubic garnet solid electrolyte of nominal composition $Li_7La_3Zr_2O_{12}$, Solid State Ionics 206 (2012) 28–32.

[20] M. Matsui, K. Sakamoto, K. Takahashi, A. Hirano, Y. Takeda, O. Yamamoto, N. Imanishi, Phase transformation of the garnet structured lithium ion conductor: $Li_7La_3Zr_2O_{12}$, Solid State Ionics 262 (2014) 155–159.

[21] R. Inada, K. Kusakabe, T. Tanaka, S. Kudo, Y. Sakurai, Synthesis and properties of Al-free $Li_{7-x}La_3Zr_{2-x}Ta_xO_{12}$ garnet related oxides, Solid State Ionics 262 (2014) 568–572.

[22] M. Hayashi, M. Takahashi, Y. Sakurai, Preparation of positive $LiCoO_2$ films by electron cyclotron resonance (ECR) plasma sputtering method and its application to all-solid-state thin-film lithium batteries, J. Power Sources 174 (2007) 990–995.

[23] N. Suzuki, S. Shirai, N. Takahashi, T. Inaba, T. Shiga, A lithium phosphorous oxynitride (LiPON) film sputtered from unsintered Li_3PO_4 powder target, Solid State Ionics 191 (2011) 49–54.

[24] D.J. Kalita, S.H. Lee, K.S. Lee, D.H. Ko, Y.S. Yoon, Ionic conductivity properties of amorphous Li–La–Zr–O solid electrolyte for thin film batteries, Solid State Ionics 229 (2012) 14–19.

[25] H. Chen, H. Tao, X. Zhao, Q. Wu, Fabrication and ionic conductivity of amorphous Li–Al–Ti–P–O thin film, J. Non-Crystalline Solids 357 (2011) 3267–3271.

[26] J. Tan, A. Tiwari, Fabrication and characterization of $Li_7La_3Zr_2O_{12}$ thin films for lithium ion battery, ECS Solid State Lett. 1 (2012) 957–960.

[27] S. Kim, M. Hirayama, S. Taminato, R. Kanno, Epitaxial growth and lithium ion

conductivity of lithium-oxide garnet for an all solid-state battery electrolyte, Dalton Trans. 42 (2013) 13112-13117.

[28] X.M. Wu, X.H. Li, S.W. Wang, Z. Wang, Y.H. Zhang ,M.F. Xu, Z. Qiang He, Preparation and characterization of lithium-ion-conductive $Li_{1.3}Al_{0.3}Ti_{1.7}(PO_4)_3$ thin films by the solution deposition, Thin Solid Films 425 (2003) 103–107.

[29] K. Takada, K. Fujimoto, T. Inada, A. Kajiyama, M. Kouguchi, S. Kondo, M. Watanabe, Sol–gel preparation of Li^+ ion conductive thin film, Appl. Surface Sci. 189 (2002) 300–306.

[30] K. Tadanaga, H. Egawa, A. Hayashi, M. Tatsumisago, J. Mosa, M. Aparicio, A. Duran, Preparation of lithium ion conductive Al-doped $Li_7La_3Zr_2O_{12}$ thin films by a sol-gel process, J. Power Sources 273 (2015) 844–847.

[31] J. Akedo, Aerosol deposition of ceramic thick films at room temperature: densification mechanism of ceramic layers, J. Am. Ceram. Soc. 89 (2006) 1834–1839.

[32] J. Akedo, M. Lebedev, Piezoelectric properties and poling effect of $Pb(Zr,Ti)O_3$ thick films prepared for microactuators by aerosol deposition, Appl. Phys. Lett. 77 (2000) 1710–1712.

[33] M. Lebedev, J. Akedo, Powder preparation in aerosol deposition method for lead zirconate titanate thick films, Jpn. J. Appl. Phys. 41-11B (2002) 6669–6673.

[34] J.H. Ryu, J. J. Choi, B.D. Hahn, D.S. Park, W.H. Yoon, and K.-H. Kim, Fabrication and ferroelectric properties of highly dense lead-free piezoelectric $(K_{0.5}Na_{0.5})NbO_3$ thick films by aerosol deposition, Appl. Phys. Lett. 90 (2007) 152901.

[35] J.H. Ryu, D.S. Park, B.D. Hahn, J.J. Choi, W.H. Yoon, K.Y. Kim, H.S. Yun, Photocatalytic TiO_2 thin films by aerosol-deposition: From micron-sized particles

to nano-grained thin film at room temperature, Appl. Catal. B Environ. 83 (2008) 1–7.

[36] W.H. Yoon, J. Ryu, J.J. Choi, B.D. Hahn, J.H. Choi, B.K. Lee, J.H. Cho, D.S. Park, Enhanced thermoelectric properties of Textured $Ca_3Co_4O_9$ thick film by aerosol deposition, J. Am. Ceram. Soc. 93 (2010) 2125–2127.

[37] D. Popovici, H. Nagai, S. Fujisima, J. Akedo, Preparation of lithium aluminum titanium phosphate electrolytes thick films by aerosol deposition method, J. Am. Ceram. Soc. 94 (2011) 3847–3850.

[38] C.W. Ahn, J.J. Choi, J. Ryu, B.D. Hahn, J.W. Kim, W.H. Yoon, J.H. Choi, D.S. Park, Microstructure and ionic conductivity in $Li_7La_3Zr_2O_{12}$ film prepared by aerosol deposition method, J. Electrochem. Soc. 162 (2015) A60–A63.

[39] H. Usui, H. Nishinami, T. Iida, H. Sakaguchi, Anode properties of Cu-coated Si thick film electrodes prepared by electroless deposition and gas-deposition, Electrochemistry 76 (2008) 329–331.

[40] H. Usui, Y. Kashiwa, T. Iida, H. Sakaguchi, Anode properties of Ru-coated Si thick film electrodes prepared by gas-deposition, J. Power Sources 195 (2010) 3649–3654.

[41] H. Usui, M. Shibata, K. Nakai, H. Sakaguchi, Anode properties of thick-film electrodes prepared by gas deposition of Ni-coated Si particles, J. Power Sources 196 (2011) 2143–2148.

[42] H. Usui, Y. Yamamoto, K. Yoshiyama, T. Itoh, H. Sakaguchi, Anode properties of composite thick-film electrodes consisted of Si and various metal silicides, J. Power Sources 196 (2011) 3911–3915.

[43] S. Takai, H. Sakaguchi, K. Tanaka, Y. Nagao, T. Esaka, Cathode performance of $LiMn_2O_4$ thick films prepared by gas-deposition for lithium rechargeable battery,

Electrochemistry 76 (2008) 293–296.

[44] I. Kim, T.H. Nam, K.W. Kim, J.H. Ahn, D.S. Park, C. Ahn, B.S. Chun, G. Wang, H.J. Ahn, $LiNi_{0.4}Co_{0.3}Mn_{0.3}O_2$ thin film electrode by aerosol deposition, Nanoscale Res. Lett. 7 (2012) 64.

[45] S. Iwasaki, T. Hamanaka, T. Yamakawa, W.C. West, K. Yamamoto, M. Motoyama, T. Hirayama, Y. Iriyama, Preparation of thick-film $LiNi_{1/3}Co_{1/3}Mn_{1/3}O_2$ electrodes by aerosol deposition and its application to all-solid-state batteries, J. Power Sources 272 (2014) 1086–1090.

[46] I. Kim, J. Park, T-H. Nam, K-W. Kim, J-H. Ahn, D-S. Park, C. Ahn, G. Wang, H-J. Ahn, Electrochemical properties of an as-deposited $LiFePO_4$ thin film electrode prepared by aerosol deposition, J. Power. Sources 244 (2013) 646–651.

[47] R. Inada, K. Shibukawa, C. Masada, Y. Nakanishi, Y. Sakurai, Characterization of as-deposited $Li_4Ti_5O_{12}$ thin film electrode prepared by aerosol deposition method, J. Power Sources 253 (2014) 181–186.

[48] C.W. Ahn, J.J. Choi, J. Ryu, B.D. Hahn, J.W. Kim, W.H. Yoon, J.H. Choi, D.S. Park, Microstructure and electrochemical properties of iron oxide film fabricated by aerosol deposition method for lithium ion battery, J. Power Sources 273 (2015) 336–340.

[49] M. Alami, R. Brochu, J.L. Soubeyroux, P. Gravereau, G. Le Flem, P. Hagenmueller, Structure and thermal expansion of $LiGe_2(PO_4)_3$, J. Solid State Chem. 90 (1991) 185–193.

Figure captions

Fig. 1. A schematic illustration of room temperature impact consolidation (RTIC) during AD.

Fig. 2. A schematic illustration of AD apparatus.

Fig. 3. The picture of aerosol deposited LAGP film on SUS316L substrate. Au electrode is deposited on the film surface.

Fig. 4. X-ray diffraction pattern (a) and SEM image (b) of as-synthesized LAGP powders. The pattern for $LiGe_2(PO_4)_3$ is also shown in (a) as the reference [49].

Fig. 5. LAGP powders pulverized with different milling time of 3 h (a) and 4.5 h (b). Both powders are used as raw materials for LAGP film fabrication by AD.

Fig. 6. X-ray diffraction patterns of aerosol deposited LAGP films using LAGP powders with different milling time: (a) 3 h (see Fig. 5(a)) and (b) 4.5 h (Fig. 5(b)). The pattern of LAGP powders is also shown in (c) as the reference.

Fig. 7. SEM images of the surface (left) and the cross-section (right) of aerosol deposited LAGP films using LAGP powders with different milling time: (a) 3 h (see Fig. 5(a)) and (b) 4.5 h (see Fig. 5(b)).

Fig. 8. Nyquist plots of AC impedance measured at 27°C for aerosol deposited LAGP films using LAGP powders with different milling time: (a) 3 h (see Fig. 5(a)) and (b) 4.5 h (Fig. 5(b)). Inset in each graph represents the enlarged data around the origin of each plot.

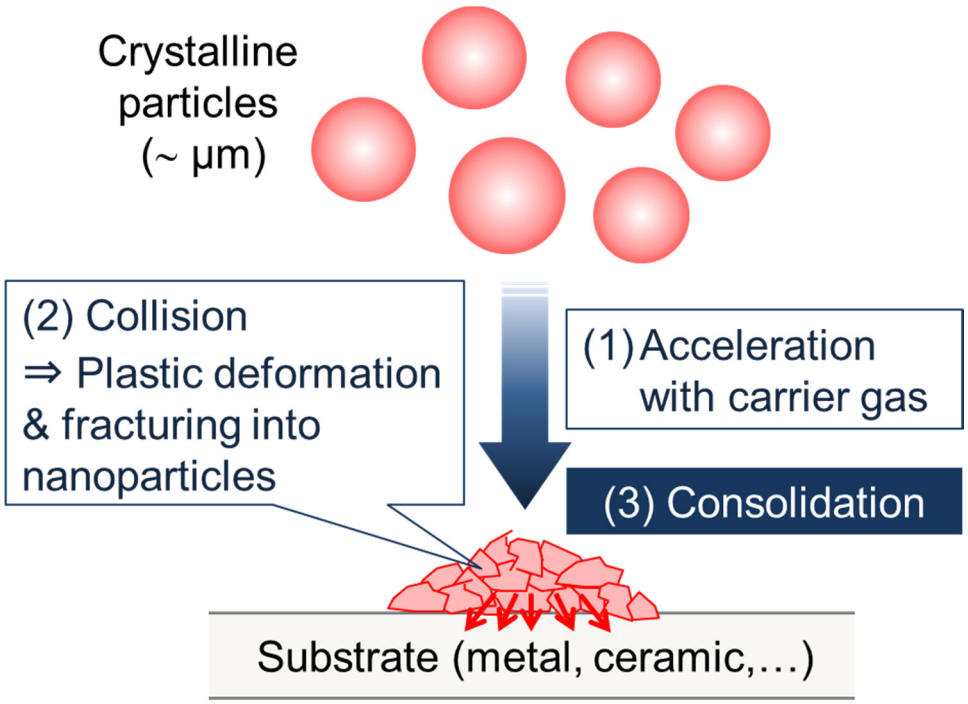
Crystalline
particles
(~ μm)
(2) Collision
⇒ Plastic deformation
& fracturing into
nanoparticles
(1) Acceleration
with carrier gas
(3) Consolidation
Substrate (metal, ceramic,…)

Fig. 1

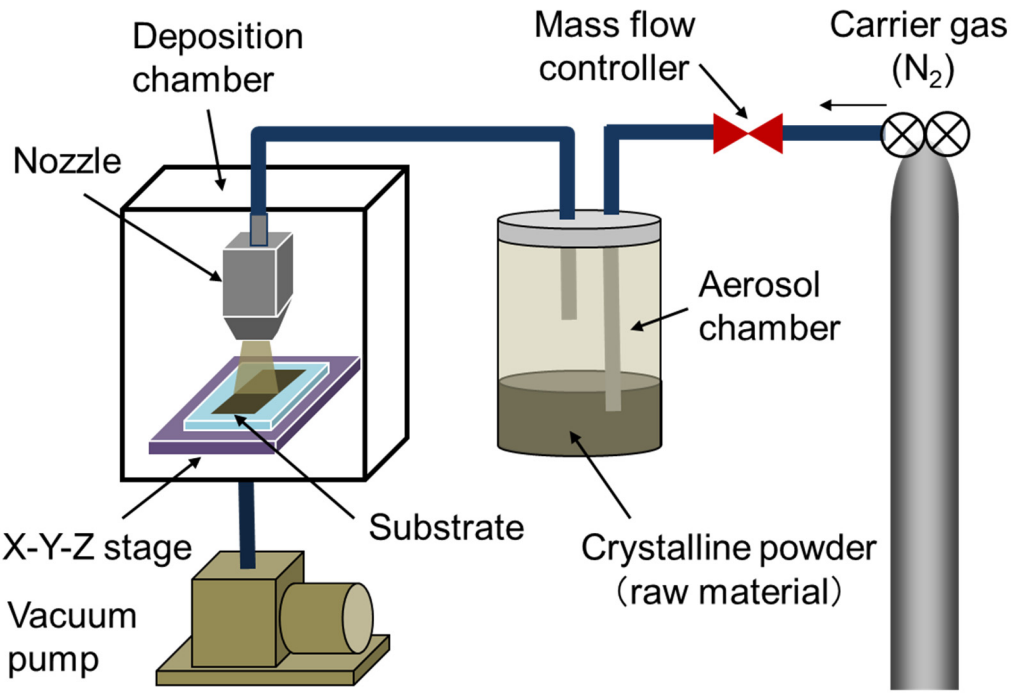
Deposition chamber
Mass flow controller
Carrier gas (N_2)
Nozzle
Aerosol chamber
Substrate
X-Y-Z stage
Crystalline powder (raw material)
Vacuum pump

Fig. 2

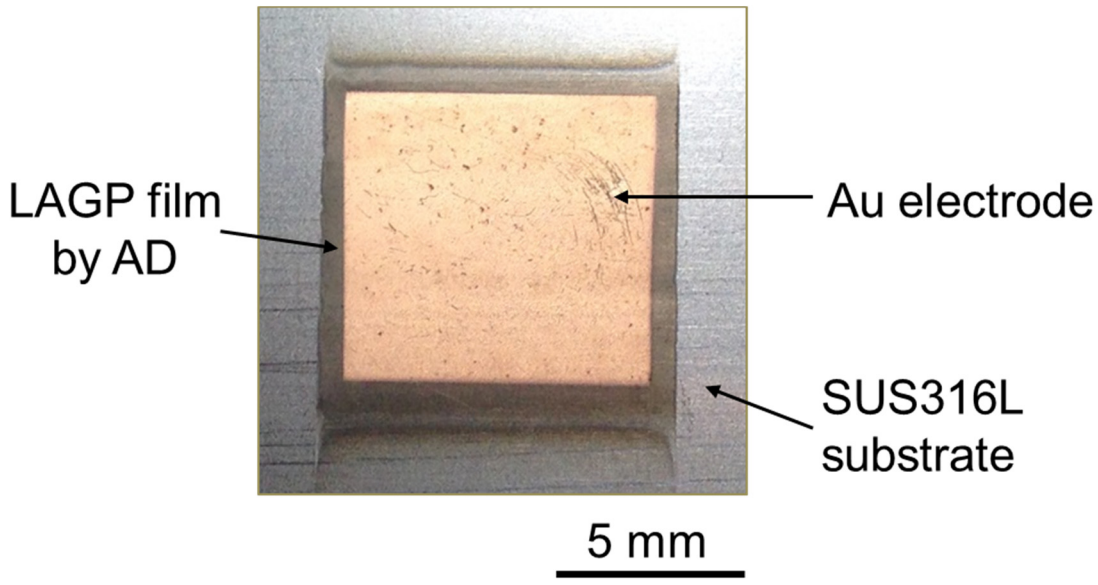

Fig. 3

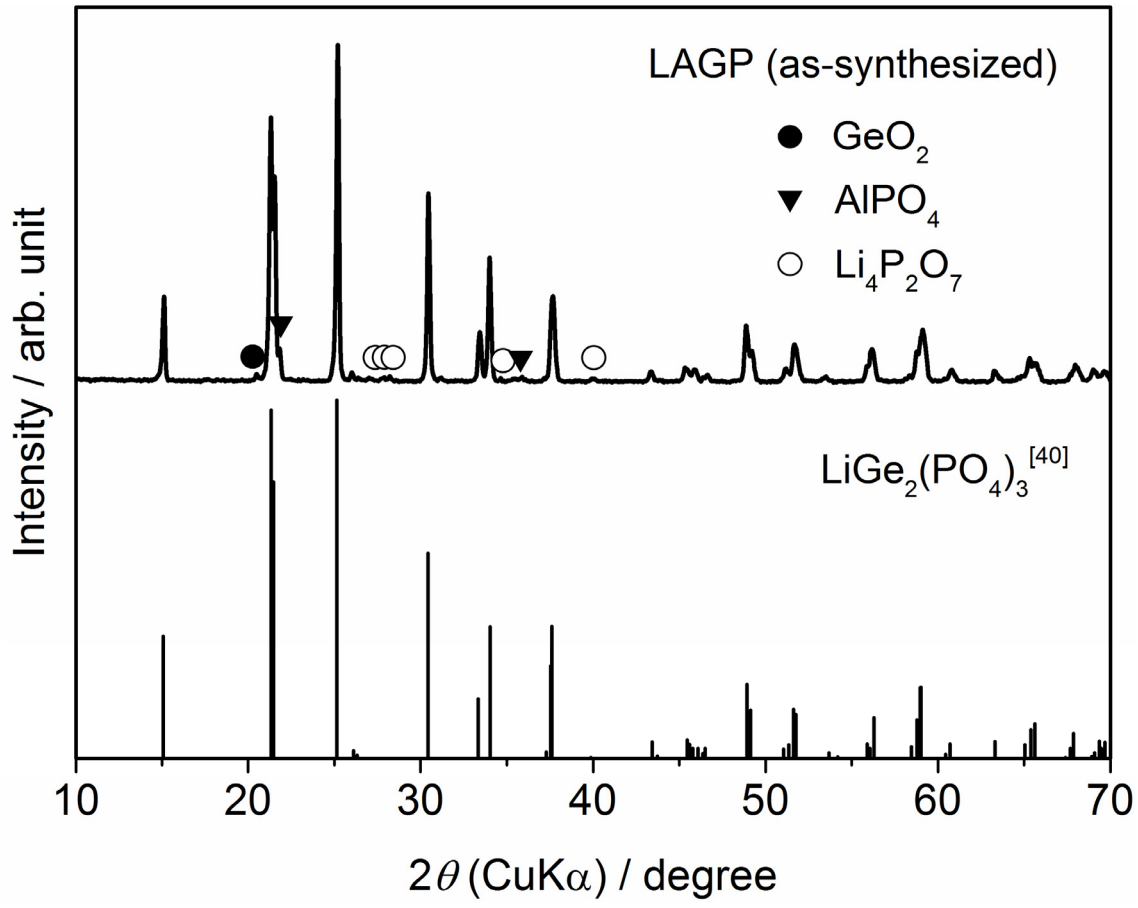
LAGP (as-synthesized)
GeO2
AlPO4
Li4P2O7
LiGe2(PO4)3 [40]
Intensity / arb. unit
10
20
30
40
50
60
70
2θ (CuKα) / degree

Fig. 4(a)

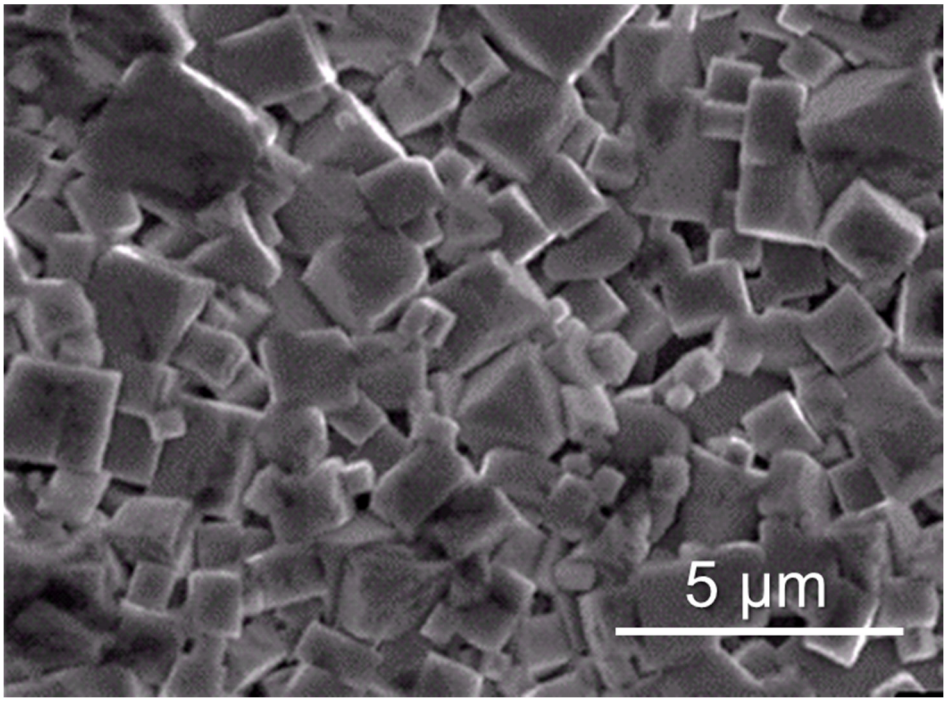

Fig. 4(b)

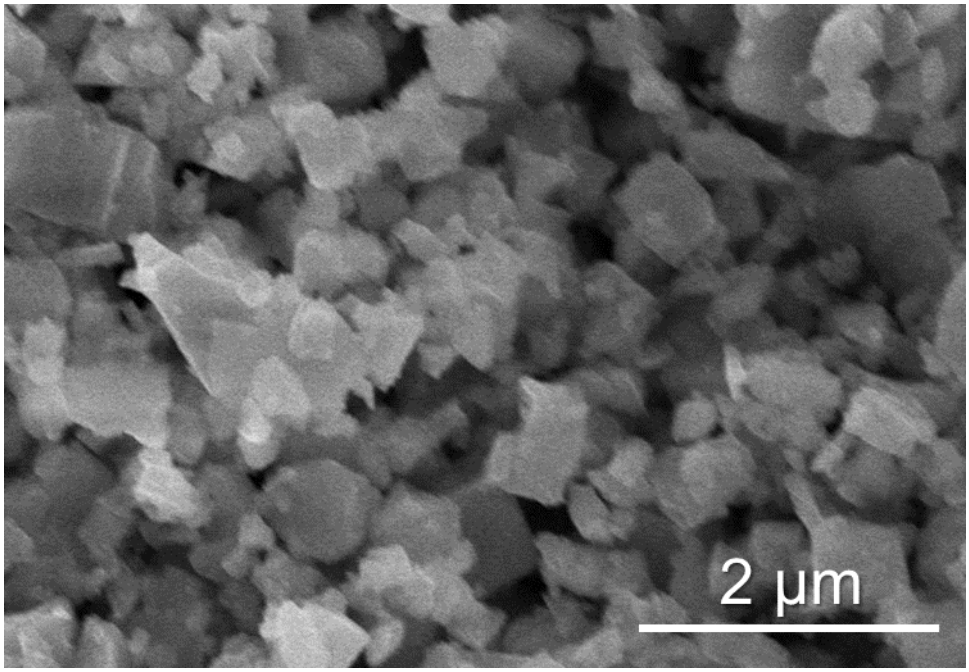

Fig. 5(a)

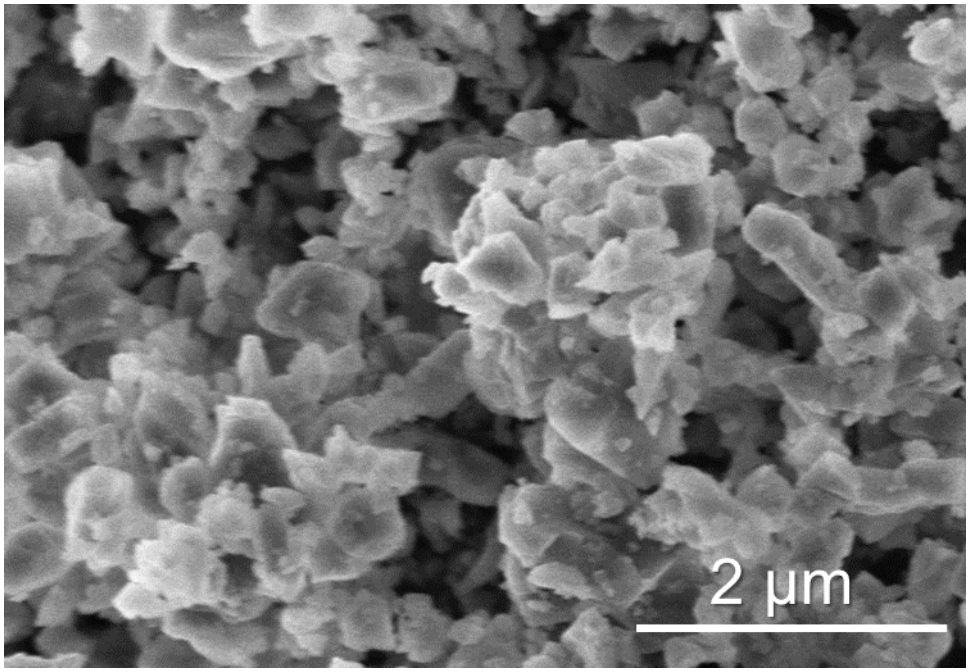

Fig. 5(b)

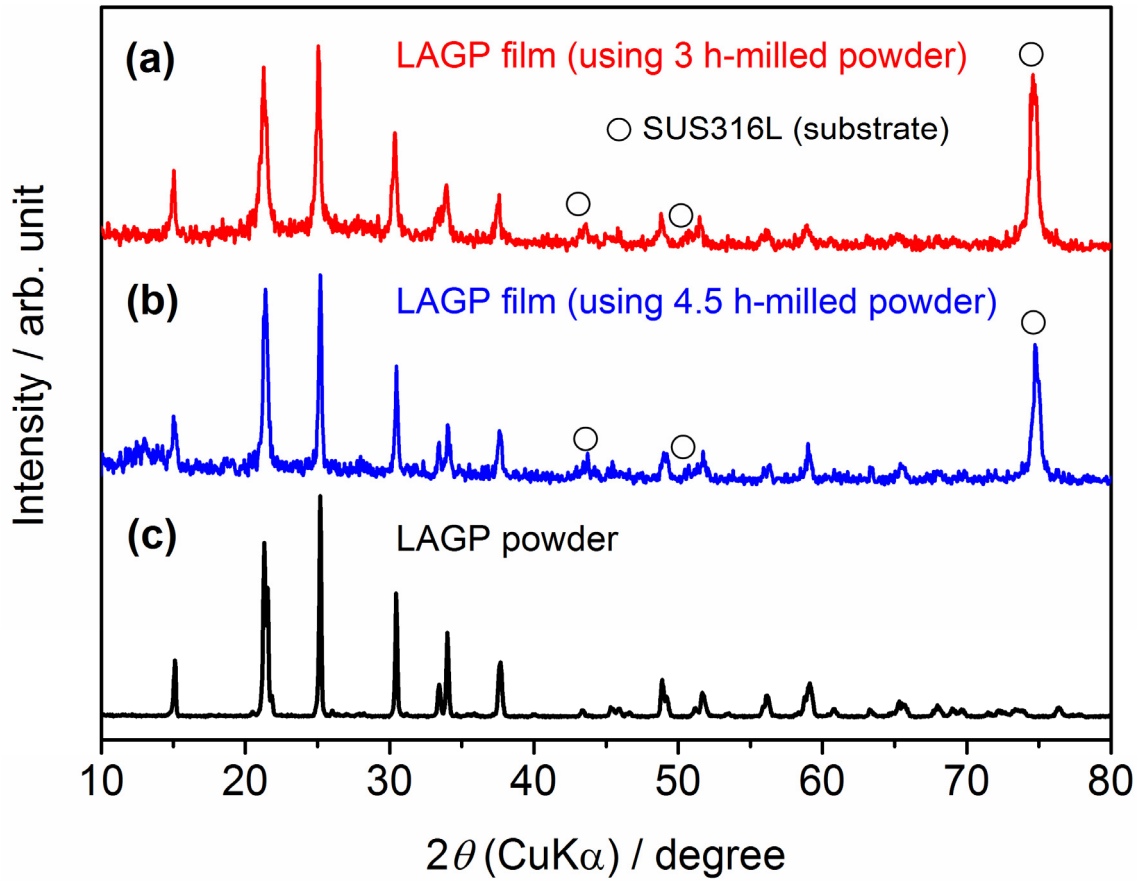
(a)
LAGP film (using 3 h-milled powder)
SUS316L (substrate)
(b)
LAGP film (using 4.5 h-milled powder)
(c)
LAGP powder
Intensity / arb. unit
10
20
30
40
50
60
70
80
2θ (CuKα) / degree

Fig. 6

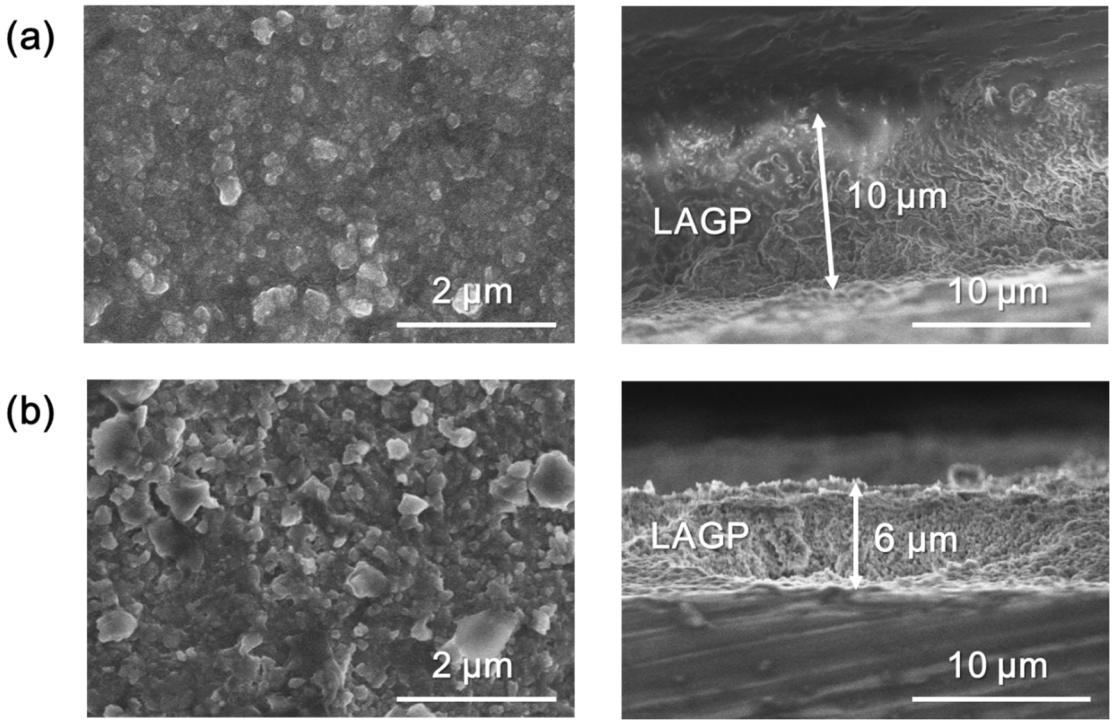

Fig. 7

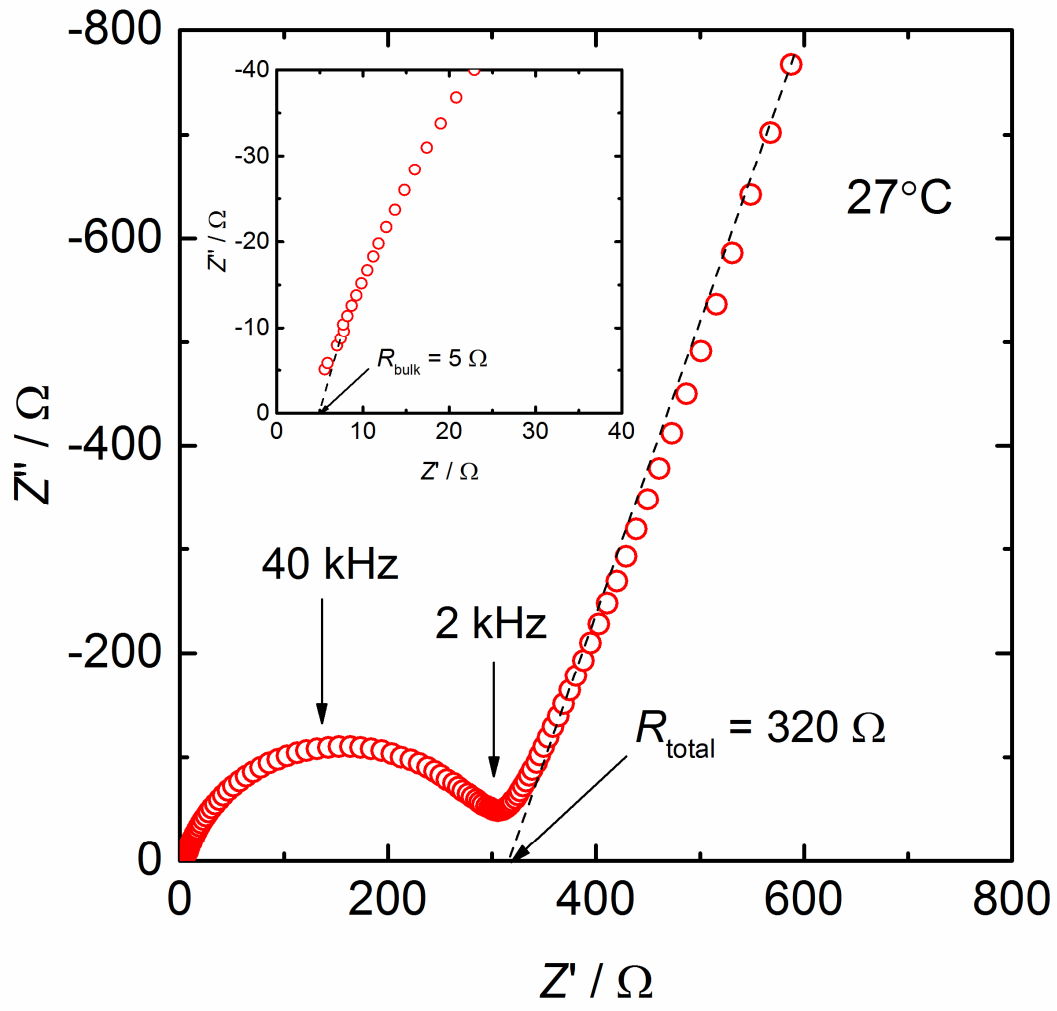
-800
-600
-400
-200
0
Z'' / Ω
0
200
400
600
800
Z' / Ω
27°C
40 kHz
2 kHz
R_total = 320 Ω
-40
-30
-20
-10
0
Z'' / Ω
0
10
20
30
40
Z' / Ω
R_bulk = 5 Ω

Fig. 8(a)

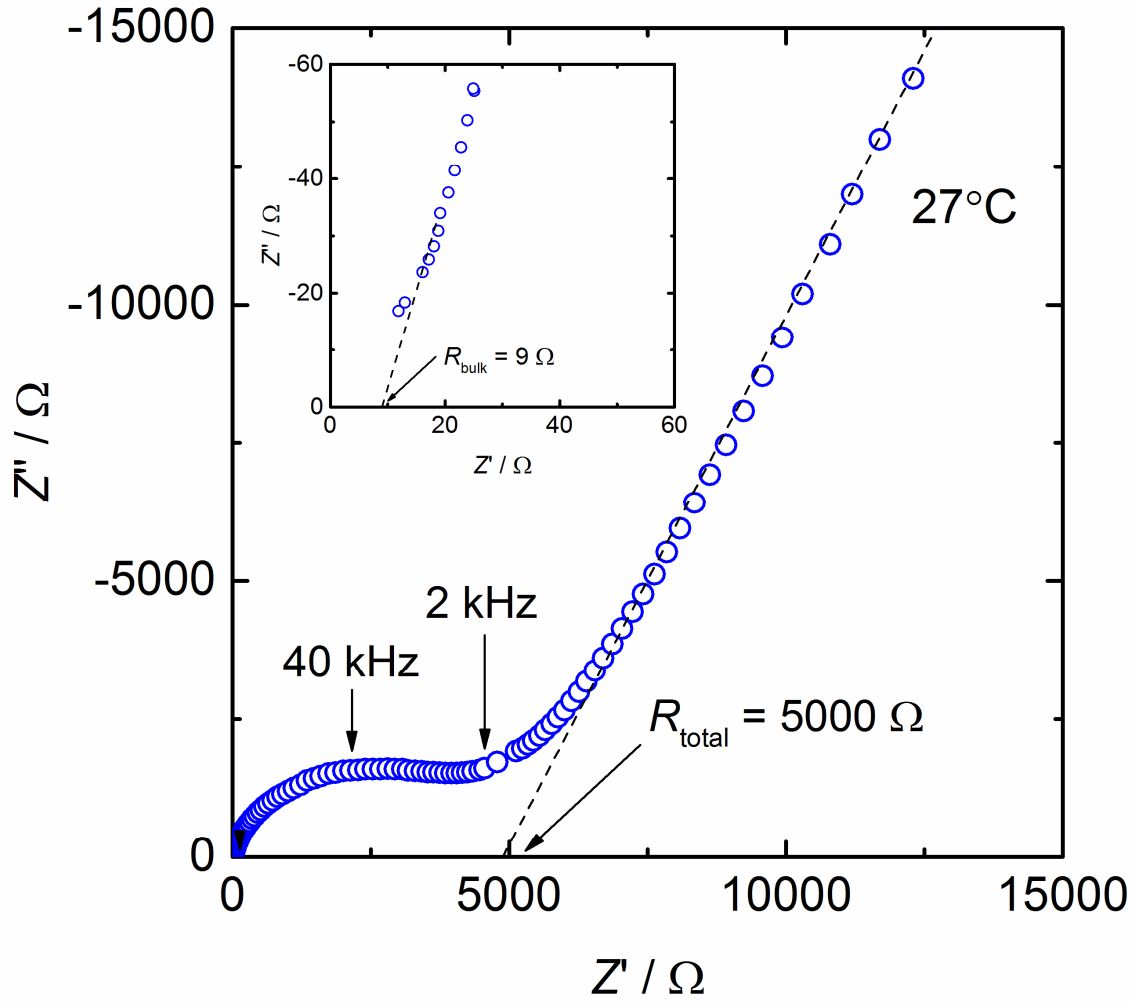
-15000
-10000
-5000
0
Z'' / Ω
0
5000
10000
15000
Z' / Ω
27°C
2 kHz
40 kHz
R_total = 5000 Ω
-60
-40
-20
0
Z'' / Ω
0
20
40
60
Z' / Ω
R_bulk = 9 Ω

Fig. 8(b)